Nanoscale Advances

ROYAL SOCIETY OF CHEMISTRY

PAPER

View Article Online
View Journal | View Issue

Cite this: *Nanoscale Adv.*, 2023, **5**, 851

$Zn_{0.4}Mg_{0.6}Fe_2O_4$ nanoenzyme: a novel chemosensitizer for the chemotherapy treatment of oral squamous cell carcinoma†

Liang Chen,‡[a] Qingmei Kong,‡[b] Mingxing Tian,[a] Qian Zhang,[b] Chengwan Xia *[b] and Chao Deng*[c]

Received 26th October 2022
Accepted 21st December 2022

DOI: 10.1039/d2na00750a

rsc.li/nanoscale-advances

Hypoxic and acidic environments are the two main components of the microenvironment contributing to the poor efficacy of chemotherapy drugs in the treatment of oral squamous cell carcinoma (OSCC). In this study, we synthesized a series of $Zn_{1-x}Mg_xFe_2O_4$ nanomaterials with enzyme-like properties, including catalase (CAT)-like, peroxidase (POD)-like, and glutathione (GSH)-like activity in an acidic environment. Among them, $Zn_{0.4}Mg_{0.6}Fe_2O_4$ performed the best and effectively increased the efficacy of doxorubicin (DOX) chemotherapy for the treatment of OSCC with reduced cardiotoxicity. Therefore, $Zn_{0.4}Mg_{0.6}Fe_2O_4$ could serve as a novel chemosensitizer in the treatment of OSCC.

1 Introduction

As one of the most malignant tumor-prone sites, the number of new cases and associated deaths due to malignant tumors in the oral cavity worldwide were 377 713 and 177 757 respectively in 2020, and the numbers are increasing every year.[1] Among these, oral squamous cell carcinoma (OSCC) accounts for 80–90%. Although radical resection is the preferred treatment, chemotherapy is still an important auxiliary method to treat or prolong life for patients with advanced/recurrence OSCC or patients who cannot tolerate surgery.[2] The armamentarium of available chemotherapy has been increasing rapidly in recent years, while the 5-year survival rate of advanced/recurrence OSCC remains less than 30%.[3,4] How to improve chemotherapy efficacy has become the key to prolonging the survival of patients with OSCC.

Hypoxic and acidic environments are two important characteristics of the tumor microenvironment. Oxygen is not only an important microenvironmental factor in the development of the organism and normal tissue homeostasis, but is also essential for oxidative metabolism, ATP production, and cell survival.[5] In the process of tumor occurrence and development, the abnormal vascular system in the tumor microenvironment leads to obstacles in oxygen delivery, and at the same time, increased oxygen consumption due to tumor cell proliferation and immune cell infiltration eventually leads to hypoxia in the tumor microenvironment.[6] Many studies have suggested that the hypoxic environment is closely related to tumor metastasis, tolerance to radiotherapy/chemotherapy, and a poor prognosis.[7,8] Moreover, the lack of oxygen in tumor tissues also leads to an increase in anaerobic glycolysis and to the production/secretion of H^+ in cells. Eventually, the acidic metabolites accumulate due to the limited blood perfusion in the acidic environment in malignant tumor tissues. Studies have shown that an acidic environment could activate proteolytic enzyme activity, which is involved in tumor tissue remodeling and tumor invasion.[9] Furthermore, the degree of acidity of tumor tissues has also been reported to be related to their degree of malignancy.[10] Therefore, this feature may be exploited as a novel approach to overcome chemotherapy tolerance in patients with OSCC by designing drugs to correct the hypoxic state based on the acidic tumor environment.

Since Yan *et al.* reported the intrinsic peroxidase-like activity of ferromagnetic nanoparticles in 2007,[11] an increasing number of nanomaterials with enzyme-like characteristics (nanozymes) have been developed and applied in the biomedical field.[12] Compared to traditional natural enzymes, nanozymes are generally of low-cost and can be mass-produced. Additionally, previous studies have shown that catalase (CAT)/peroxidase (POD) mimic nanozymes such as $MnFe_2O_4$ could catalyze H_2O_2 oxygen production, which could correct the hypoxic state in tumor tissue and may produce reactive oxygen species (ROS) that could inhibit tumor cell proliferation.[13–15] This suggests that we may be able to correct the hypoxic state by constructing appropriate nanozymes that reduce tolerance to chemotherapy in OSCC patients.

[a]*Department of Oral and Maxillofacial Surgery, Yi Ji Shan Hospital of Wannan Medical College, Wuhu, Anhui, China*

[b]*Department of Oral and Maxillofacial Surgery, Nanjing Stomatology Hospital, Medical School of Nanjing University, Nanjing, China. E-mail: 2665927917@qq.com*

[c]*Key Laboratory of Non-coding RNA Transformation Research of Anhui Higher Education, School of Stomatology, Wannan Medical College, Anhui, China. E-mail: 20120015@wnmc.edu.cn*

† Electronic supplementary information (ESI) available. See DOI: https://doi.org/10.1039/d2na00750a

‡ These authors contributed equally to this article.

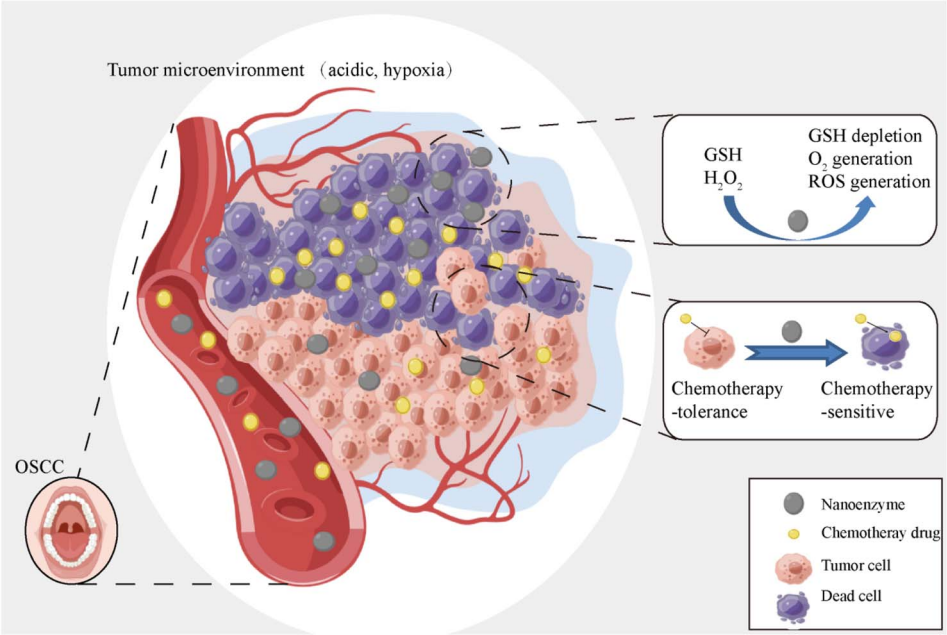

Fig. 1 Diagram of the chemosensitization mechanism of the $Zn_{0.4}Mg_{0.6}Fe_2O_4$ nanoenzyme.

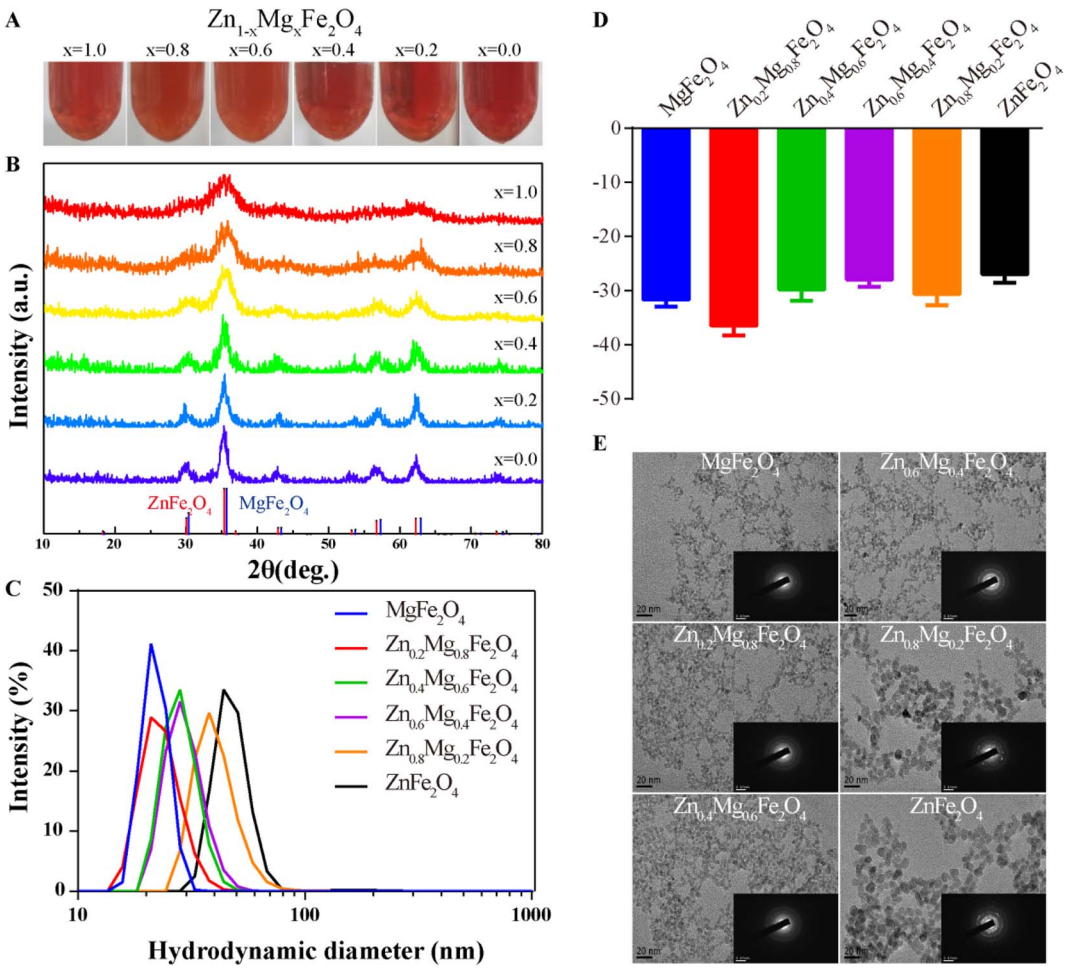

Fig. 2 Characterization of $Zn_{1-x}Mg_xFe_2O_4$. (A) Camera images of $Zn_{1-x}Mg_xFe_2O_4$, (B) XRD spectra of $Zn_{1-x}Mg_xFe_2O_4$, (C) DLS of $Zn_{1-x}Mg_xFe_2O_4$, (D) zeta potential of $Zn_{1-x}Mg_xFe_2O_4$ and (E) TEM images of $Zn_{1-x}Mg_xFe_2O_4$, and the insets show the SAED patterns, respectively.

In this paper, a series of $Zn_{1-x}Mg_xFe_2O_4$ nanozymes were synthesized and, of these, $Zn_{0.4}Mg_{0.6}Fe_2O_4$ exhibited the highest catalytic efficiency of POD-like, CAT-like, and GSH-like activity. Furthermore, the properties of POD–CAT and glutathione (GSH) activity of $Zn_{0.4}Mg_{0.6}Fe_2O_4$ were verified *in vitro*. Finally, we verified whether $Zn_{0.4}Mg_{0.6}Fe_2O_4$ could reduce chemotherapy tolerance and improve the effect of chemotherapy on OSCC, and the results showed that $Zn_{0.4}Mg_{0.6}Fe_2O_4$ could serve as a promising chemosensitizer in OSCC management. The main scheme of our study is depicted below (Fig. 1).

2 Results and discussion

2.1 Synthesis and characterization of $Zn_{1-x}Mg_xFe_2O_4$

A series of $Zn_{1-x}Mg_xFe_2O_4$ molecules were successfully synthesized as shown in Fig. 2A and the X-ray diffraction (XRD) spectra are given in Fig. 2B. Their hydrodynamic diameters measured by dynamic light scattering (DLS) were 21.96 ± 3.10 nm ($MgFe_2O_4$, polymer dispersity index (PDI): 0.02), 23.41 ± 5.04 nm ($Zn_{0.2}Mg_{0.8}Fe_2O_4$, PDI: 0.05), 28.52 ± 5.36 nm ($Zn_{0.4}Mg_{0.6}Fe_2O_4$, PDI: 0.04), 29.67 ± 6.24 nm ($Zn_{0.6}Mg_{0.4}Fe_2O_4$, PDI: 0.04), 40.80 ± 9.76 nm ($Zn_{0.8}Mg_{0.2}Fe_2O_4$, PDI: 0.06), and 48.70 ± 15.43 nm ($ZnFe_2O_4$, PDI: 0.10), as shown in Fig. 2C. The diameter of $Zn_{1-x}Mg_xFe_2O_4$ increased with an increase in the Zn ratio. The zeta potentials of obtained $Zn_{1-x}Mg_xFe_2O_4$ were −31.63 ± 1.31 mV ($MgFe_2O_4$), −36.5 ± 1.75 mV ($Zn_{0.2}Mg_{0.8}Fe_2O_4$), −29.83 ± 2.05 mV ($Zn_{0.4}Mg_{0.6}Fe_2O_4$), −27.93 ± 1.34 mV ($Zn_{0.6}Mg_{0.4}Fe_2O_4$), −30.63 ± 2.11 mV ($Zn_{0.8}Mg_{0.2}Fe_2O_4$), and −26.93 ± 1.57 mV ($ZnFe_2O_4$), as shown in Fig. 2D. The morphology was evaluated using a transmission electron microscope (TEM) and the selected area electron diffraction (SAED) showed that these nanoparticles had a morphology of homogeneously dispersed spheres and a single-crystal structure, as shown in Fig. 2E.

2.2 CAT-like, POD-like, and GSH-like properties of $Zn_{1-x}Mg_xFe_2O_4$

2.2.1 $Zn_{0.4}Mg_{0.6}Fe_2O_4$ exhibited excellent CAT-like activity. It is effective in reducing the tolerance to OSCC chemotherapy by increasing the content of O_2. As shown in Fig. 3A, H_2O_2 was abundant in OSCC tumor tissues compared to normal tissues, which could provide the substrate for the generation of O_2. Therefore, both the consumption of H_2O_2 and the generation of O_2 have been used to assess the CAT-like activity of $Zn_{1-x}Mg_xFe_2O_4$. In terms of consumption of H_2O_2, $Zn_{0.4}Mg_{0.6}Fe_2O_4$, $Zn_{0.8}Mg_{0.2}Fe_2O_4$, and $ZnFe_2O_4$ showed CAT-like activity in an acid/neutral environment (pH = 5.8/7.4) compared to the control group, while $Zn_{0.6}Mg_{0.4}Fe_2O_4$, $Zn_{0.2}Mg_{0.8}Fe_2O_4$, and $MgFe_2O_4$ did not (Fig. 3B, C and S1†). The amount of H_2O_2 consumption at 3 h was used to explore the influence of the Zn/Mg ratio on the CAT-like catalytic efficiency of $Zn_{1-x}Mg_xFe_2O_4$. As shown in Fig. 3D, $Zn_{0.4}Mg_{0.6}Fe_2O_4$ has decomposed the maximum amount of H_2O_2 than the other $Zn_{1-x}Mg_xFe_2O_4$ nanozymes. Furthermore, as shown in Fig. 3E, $Zn_{0.4}Mg_{0.6}Fe_2O_4$ was also the O_2-producing $Zn_{1-x}Mg_xFe_2O_4$. Therefore,

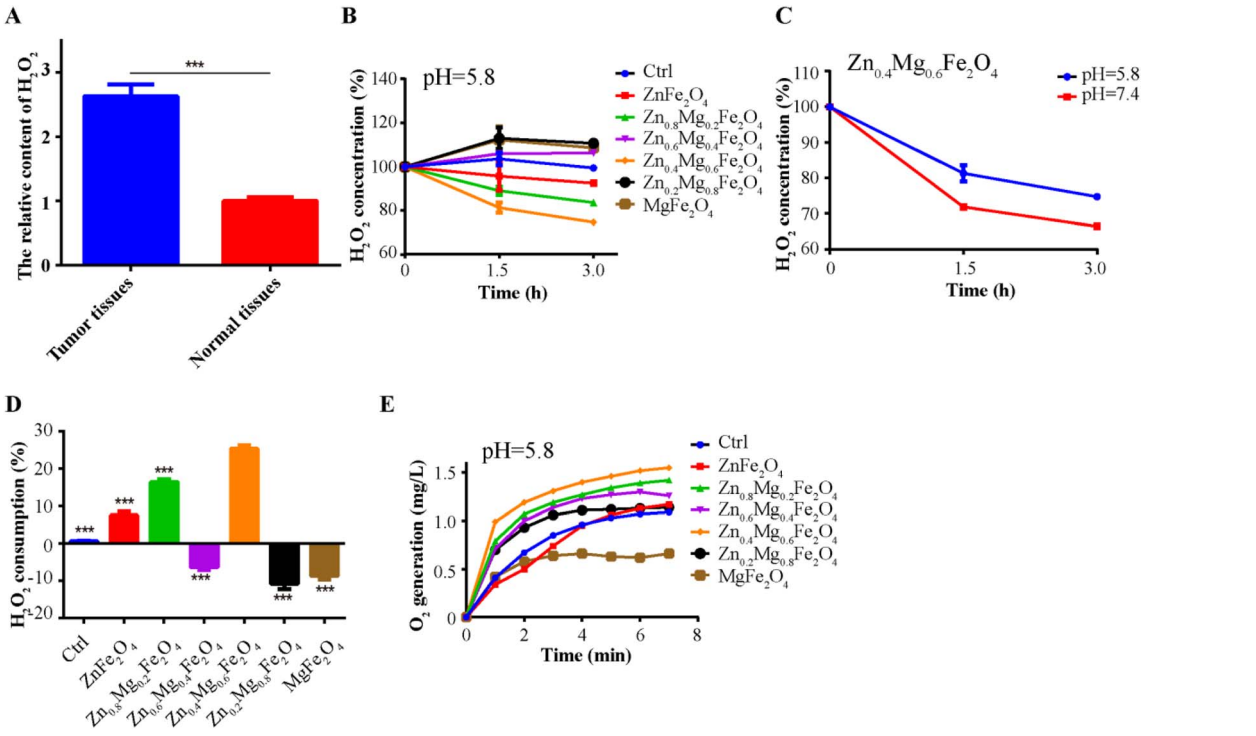

Fig. 3 Properties of the CAT-like activity of $Zn_{0.4}Mg_{0.6}Fe_2O_4$. (A) The H_2O_2 content in OSCC tumor tissues and normal tissues. (B) H_2O_2 consumption continues after treatment with $Zn_{1-x}Mg_xFe_2O_4$ in an acidic environment. (C) Continuous consumption of H_2O_2 after treatment with $Zn_{0.4}Mg_{0.6}Fe_2O_4$ in different buffers (PBS, pH = 5.8 or 7.4). (D) Comparison of CAT-like activity at 3 h. (E) Continuous generation of O_2 after treatment with $Zn_{1-x}Mg_xFe_2O_4$ in an acidic environment. ***: $P < 0.001$.

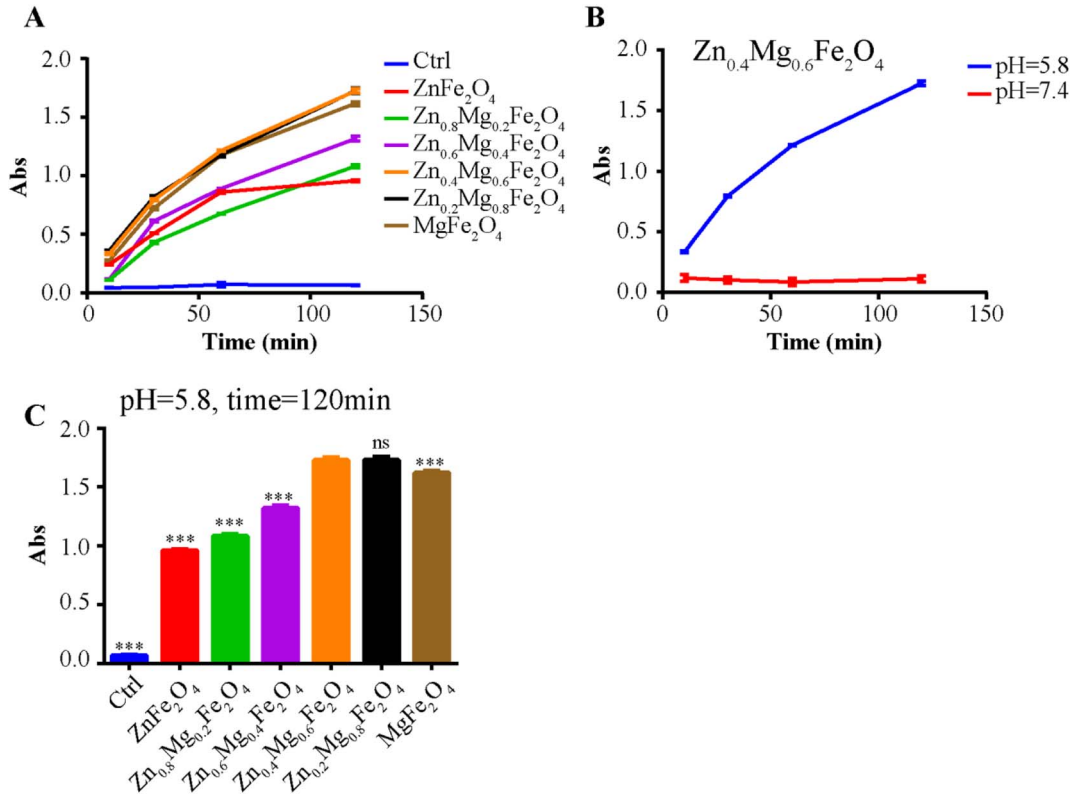

Fig. 4 POD-like activity of $Zn_{0.4}Mg_{0.6}Fe_2O_4$. (A) ROS generation after treatment with $Zn_{1-x}Mg_xFe_2O_4$ in an acidic environment. (B) Continuous ROS generation after treatment with $Zn_{0.4}Mg_{0.6}Fe_2O_4$ in different buffers (PBS, pH = 5.8 or 7.4). (C) Comparison of CAT-like activity at 120 min in an acidic environment.

$Zn_{0.4}Mg_{0.6}Fe_2O_4$ has potential application value in correcting the tumor hypoxic microenvironment of OSCC and improving the chemotherapy effect.

2.2.2 $Zn_{0.4}Mg_{0.6}Fe_2O_4$ exhibited excellent POD-like activity. ROS detection was performed to investigate the POD-like activity of $Zn_{1-x}Mg_xFe_2O_4$. As shown in Fig. 4A, B and S2,† compared to the control group, all $Zn_{1-x}Mg_xFe_2O_4$ exhibited POD-like activity in an acid environment (pH = 5.8), and no POD-like activity was observed in a neutral environment (pH = 7.4). The acid response of the POD-like activity of $Zn_{1-x}Mg_xFe_2O_4$ ensured that the nanoenzyme would kill tumor cells only in the acidic tumor microenvironment, but would not damage normal cells. To further explore the influence of the Zn/Mg ratio on the POD-like catalytic efficiency of $Zn_{1-x}Mg_xFe_2O_4$, the catalytic efficiency at 120 min was compared. As shown in Fig. 4C, the POD-like catalytic efficiency presented an earlier increasing and later decreasing trend with an increase of the Mg ratio; $Zn_{0.4}Mg_{0.6}Fe_2O_4$ and $Zn_{0.2}Mg_{0.8}Fe_2O_4$ had the highest POD-like catalytic efficiency.

2.2.3 $Zn_{0.4}Mg_{0.6}Fe_2O_4$ exhibited excellent GSH-like activity in an acid environment. Given the high H_2O_2 levels, OSCC also contained a large amount of GSH compared to normal tissues, which would increase the occurrence of chemotherapy tolerance.[16–18] Furthermore, previous research indicated that Fe^{3+} could be reduced to Fe^{2+} by GSH and Fe^{2+} could further convert H_2O_2 to O_2 or ROS.[19] Therefore, the GSH-like activity of $Zn_{1-x}Mg_xFe_2O_4$ was evaluated by detecting GSH consumption, Fe^{2+} generation, and Fe^{3+} depletion. As shown in Fig. 5A, GSH has been significantly consumed by $Zn_{0.4}Mg_{0.6}Fe_2O_4$ (14% at 6 h and 24% at 12 h) in an acidic environment. Furthermore, the generation of Fe^{2+} was also positively correlated with the concentration of $Zn_{0.4}Mg_{0.6}Fe_2O_4$ in an acid environment, while very little Fe^{2+} was generated in a neutral environment as shown in Fig. 5B, C and S3.† Furthermore, Fe^{3+} has also obviously been depleted after culture with GSH in acidic buffer, as shown in Fig. 5D. In summary, $Zn_{0.4}Mg_{0.6}Fe_2O_4$ exhibited the best enzyme-like activity among the $Zn_{1-x}Mg_xFe_2O_4$ nanozymes which would increase sensitivity to chemotherapy.

2.3 $Zn_{0.4}Mg_{0.6}Fe_2O_4$ could shape the tumor microenvironment that inhibits the progression of OSCC

To further validate the CAT-like activity of $Zn_{0.4}Mg_{0.6}Fe_2O_4$ *in vitro*, the levels of H_2O_2 and HIF-1α were detected in OSCC tumor cells treated with 100 μg mL^{-1} $Zn_{0.4}Mg_{0.6}Fe_2O_4$. As shown in Fig. 6A, compared to the normoxic environment, the H_2O_2 content was markedly elevated in tumor cells cultured in a hypoxic environment, and was also depleted after treatment with $Zn_{0.4}Mg_{0.6}Fe_2O_4$. The expression of HIF-1α reflected the O_2 content in the cells. As shown in Fig. 6B, the expression of HIF-1α in tumor cells cultured in a hypoxic environment was significantly higher than that in a normoxic environment and also decreased after treatment with $Zn_{0.4}Mg_{0.6}Fe_2O_4$. The ROS content was detected to validate the POD activity of

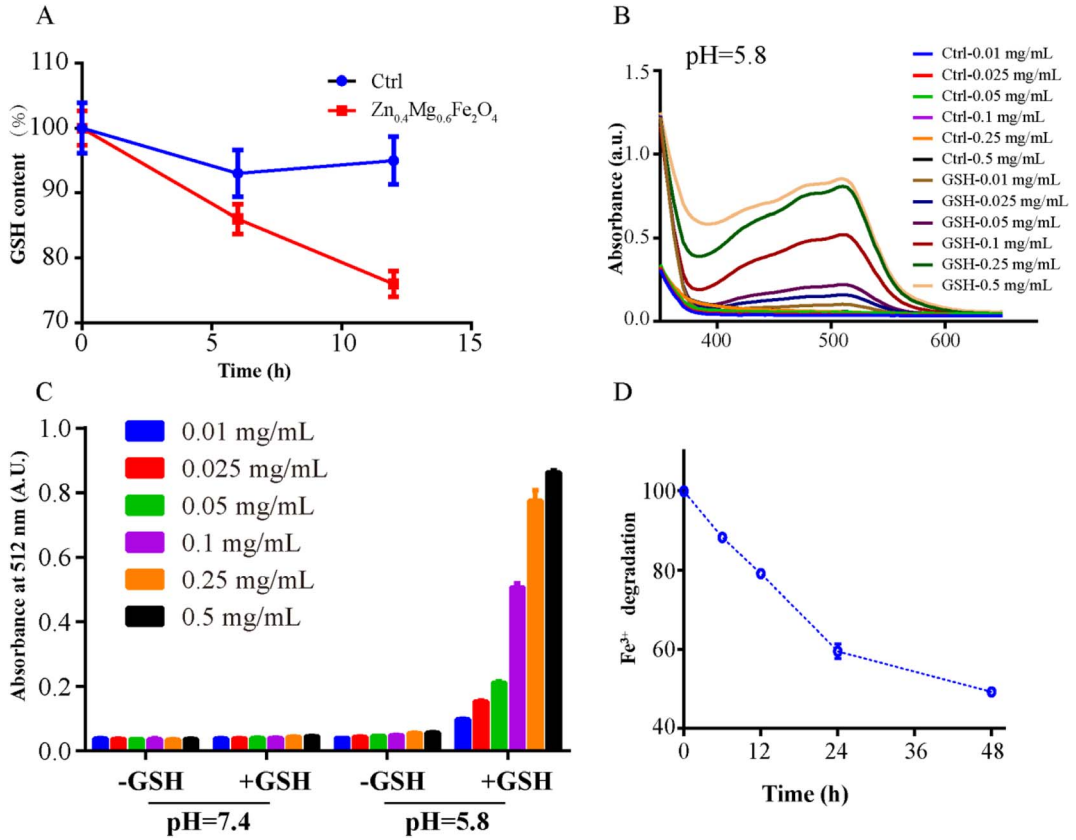

Fig. 5 Properties of the GSH-like activity of $Zn_{0.4}Mg_{0.6}Fe_2O_4$. (A) GSH consumption after treatment with $Zn_{0.4}Mg_{0.6}Fe_2O_4$ in an acidic environment. (B) Fe^{2+} generation after treating with different concentrations of $Zn_{0.4}Mg_{0.6}Fe_2O_4$ in an acidic environment. (C) Fe^{2+} generation after treating with different concentrations of $Zn_{0.4}Mg_{0.6}Fe_2O_4$ in acidic and neutral environments. (D) Depletion of Fe^{3+} after treatment with $Zn_{0.4}Mg_{0.6}Fe_2O_4$.

$Zn_{0.4}Mg_{0.6}Fe_2O_4$ *in vitro*. As shown in Fig. 6C, the ROS content in tumor cells was increased both in a normaxic and a hypoxic environment after treatment with $Zn_{0.4}Mg_{0.6}Fe_2O_4$., which further demonstrated that $Zn_{0.4}Mg_{0.6}Fe_2O_4$ also exhibited excellent enzyme-like activity in cells. Subsequently, a cell wound scratch assay and a transwell cell migration assay were performed to evaluate the influence of $Zn_{0.4}Mg_{0.6}Fe_2O_4$ on OSCC tumor cells. As shown in Fig. 6D and E, the migration rate of tumor cells increased significantly in the hypoxic environment compared to the normoxic environment, while the migration rate also decreased after treating with $Zn_{0.4}Mg_{0.6}Fe_2O_4$. This means that $Zn_{0.4}Mg_{0.6}Fe_2O_4$ may inhibit the progression of OSCC through an appropriate hypoxia environment.

2.4 $Zn_{0.4}Mg_{0.6}Fe_2O_4$ could improve the chemotherapy effect in OSCC

In addition to surgery, chemotherapy is also an important treatment for OSCC. However, due to the tolerance to chemotherapy caused by various factors, such as hypoxia, chemotherapy outcomes are still less than satisfactory. A chemosensitizer could enhance the effect of chemotherapy. Therefore, $Zn_{0.4}Mg_{0.6}Fe_2O_4$ was combined with DOX (first-line chemotherapy for OSCC) to treat OSCC in this study. First, the CCK-8 assay was performed to evaluate the toxicity of $Zn_{0.4}Mg_{0.6}Fe_2O_4$ to OSCC cells. As shown in Fig. 7A and B, cell viability decreased as the concentration of $Zn_{0.4}Mg_{0.6}Fe_2O_4$ increased in an acidic environment (IC_{50}-$Zn_{0.4}Mg_{0.6}Fe_2O_4$: 1.398 mg mL^{-1}) while no toxicity was observed in a neutral environment. Furthermore, the live/dead cell-double staining assay also showed greater OSCC cell death after treatment with 0.1 mg mL^{-1} $Zn_{0.4}Mg_{0.6}Fe_2O_4$ in an acidic environment, as shown in Fig. 7C, which indicated that the lethal effect of $Zn_{0.4}Mg_{0.6}Fe_2O_4$ also had acid-response properties *in vitro*. Subsequently, we further evaluated whether $Zn_{0.4}Mg_{0.6}Fe_2O_4$ could enhance the chemotherapy effect of DOX on OSCC cells. As shown in Fig. 7D, compared to DOX alone (IC_{50}-DOX: 0.737 mg mL^{-1}), OSCC cell viability obviously decreased when combined with 0.1 mg mL^{-1} $Zn_{0.4}Mg_{0.6}Fe_2O_4$ (IC_{50}-DOX and $Zn_{0.4}Mg_{0.6}Fe_2O_4$: 0.394 mg mL^{-1} and 0.1 mg mL^{-1}, combination index: 0.616). Thus, $Zn_{0.4}Mg_{0.6}Fe_2O_4$ could efficiently enhance the chemotherapy effect of DOX on OSCC cells. Finally, a mouse xenograft OSCC tumor model was used to further validate our findings *in vivo*. As shown in Fig. 7E and F, the tumor volume of mice injected with $Zn_{0.4}Mg_{0.6}Fe_2O_4$ and DOX was significantly lower than that of mice injected with DOX alone, while the body weight of mice injected with $Zn_{0.4}Mg_{0.6}Fe_2O_4$ and DOX was higher as shown in Fig. 7G. Furthermore,

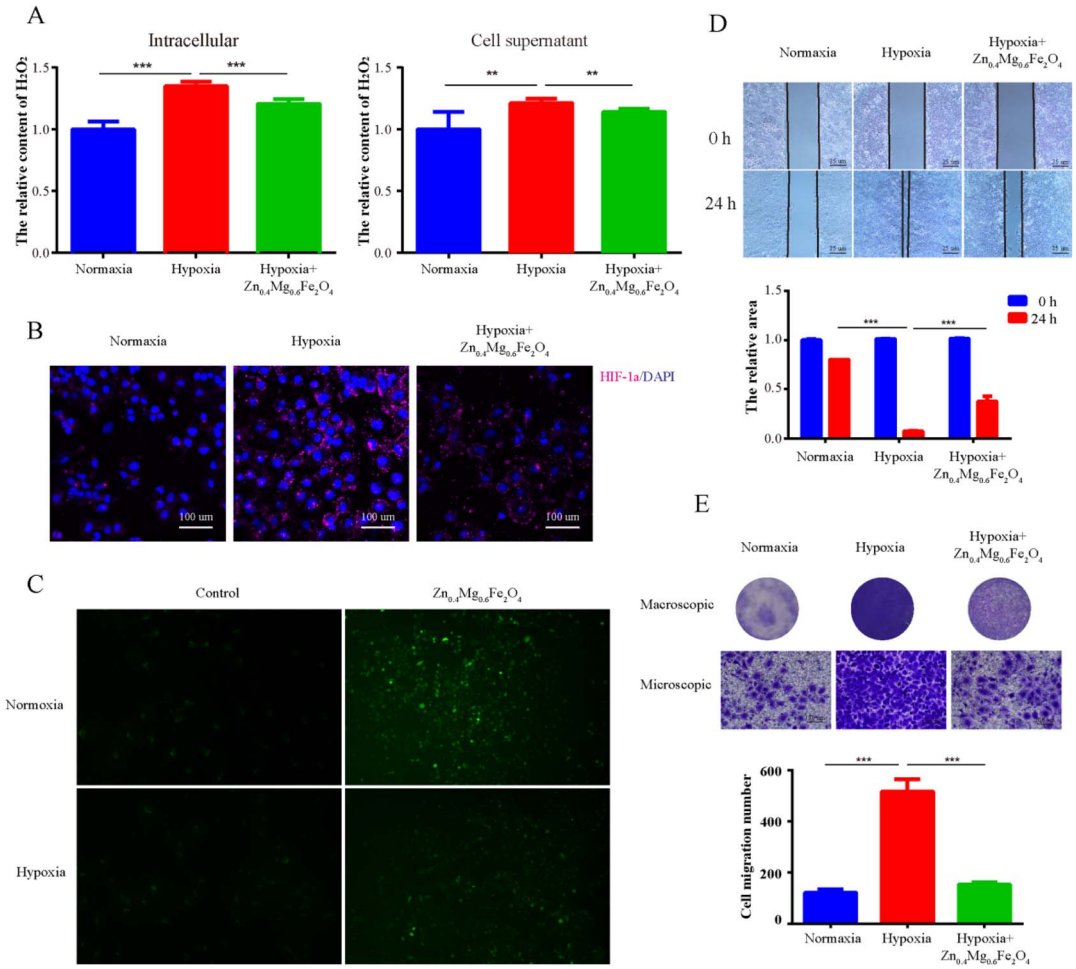

Fig. 6 The influence of $Zn_{0.4}Mg_{0.6}Fe_2O_4$ on OSCC. (A) The effect of $Zn_{0.4}Mg_{0.6}Fe_2O_4$ on the H_2O_2 content, (B) on the expression of HIF-1α, (C) on ROS generation, and (D-E) on the migration ability of OSCC cells. **: $P < 0.01$, ***: $P < 0.001$.

cardiotoxicity was also less marked in mice injected with $Zn_{0.4}Mg_{0.6}Fe_2O_4$ compared to mice injected with DOX alone (Fig. 7H). Thus, $Zn_{0.4}Mg_{0.6}Fe_2O_4$ can not only enhance DOX chemotherapy, but can also efficiently reduce the toxicity of DOX chemotherapy *in vivo*. Therefore, $Zn_{0.4}Mg_{0.6}Fe_2O_4$ could serve as a chemo-sensitizer in the management of OSCC.

3 Experimental section

3.1 Synthesis of $Zn_{1-x}Mg_xFe_2O_4$ nanozymes

The $Zn_{1-x}Mg_xFe_2O_4$ nanozymes were prepared according to previously reported protocols with minor modifications.[20,21] Specifically, 0.05 M $Mg(NO_3)_2{\cdot}6H_2O$/$Zn(NO_3)_2{\cdot}6H_2O$ (the ratio between $Mg(NO_3)_2{\cdot}6H_2O$ and $Zn(NO_3)_2{\cdot}6H_2O$ was established according to the stoichiometry of $Zn_{1-x}Mg_xFe_2O_4$), 0.1 M $Fe(NO_3)_3$ $9H_2O$ and 0.15 M trisodium citrate were dissolved in 190 mL of distilled water and 10 mL of 1 M NaOH solution was then slowly added to the solution. The reactants were then placed in a 500-mL capacity container in a Teflon-lined autoclave. The autoclave was maintained at 160 °C for 6 h to prepare $MgFe_2O_4$, 180 °C for 8 h to prepare $Zn_{0.2}Mg_{0.8}Fe_2O_4$ and $Zn_{0.4}Mg_{0.6}Fe_2O_4$, and 180 °C for 6 h to prepare $Zn_{0.6}Mg_{0.4}Fe_2O_4$, $Zn_{0.8}Mg_{0.2}Fe_2O_4$, and $ZnFe_2O_4$.

3.2 Characterization of $Zn_{1-x}Mg_xFe_2O_4$ nanozymes

The structural characterization and phase identifications of the sample are done with an X-ray diffractometer (Bruker AKS D8 Advance). The hydrodynamic diameter and zeta potential were measured using a dynamic light scattering instrument (DLS) (ZetaSizer Nano-ZS90; Malvern Instrument) in zeta potential analysis mode. The size and morphology of the obtained $Zn_{1-x}Mg_xFe_2O_4$ nanozymes were observed by transmission electron microscopy (TEM; JEOL).

3.3 H_2O_2 consumption

The H_2O_2 consumption was measured using the colorimetric method of titanium sulfate ($Ti(SO_4)_2$) according to a previous protocol with minor modifications.[22] Specifically, solution A: 2 mg of $Zn_{1-x}Mg_xFe_2O_4$ was incubated with 5 mL of H_2O_2 (1 mM) in different buffers (pH 7.4 or pH 5.8) and stirred at 37 °C. Solution B: 665 μL of $Ti(SO_4)_2$ and 4.165 mL of H_2SO_4 were mixed with 25 mL of water. Then 100 μL of solution A was added

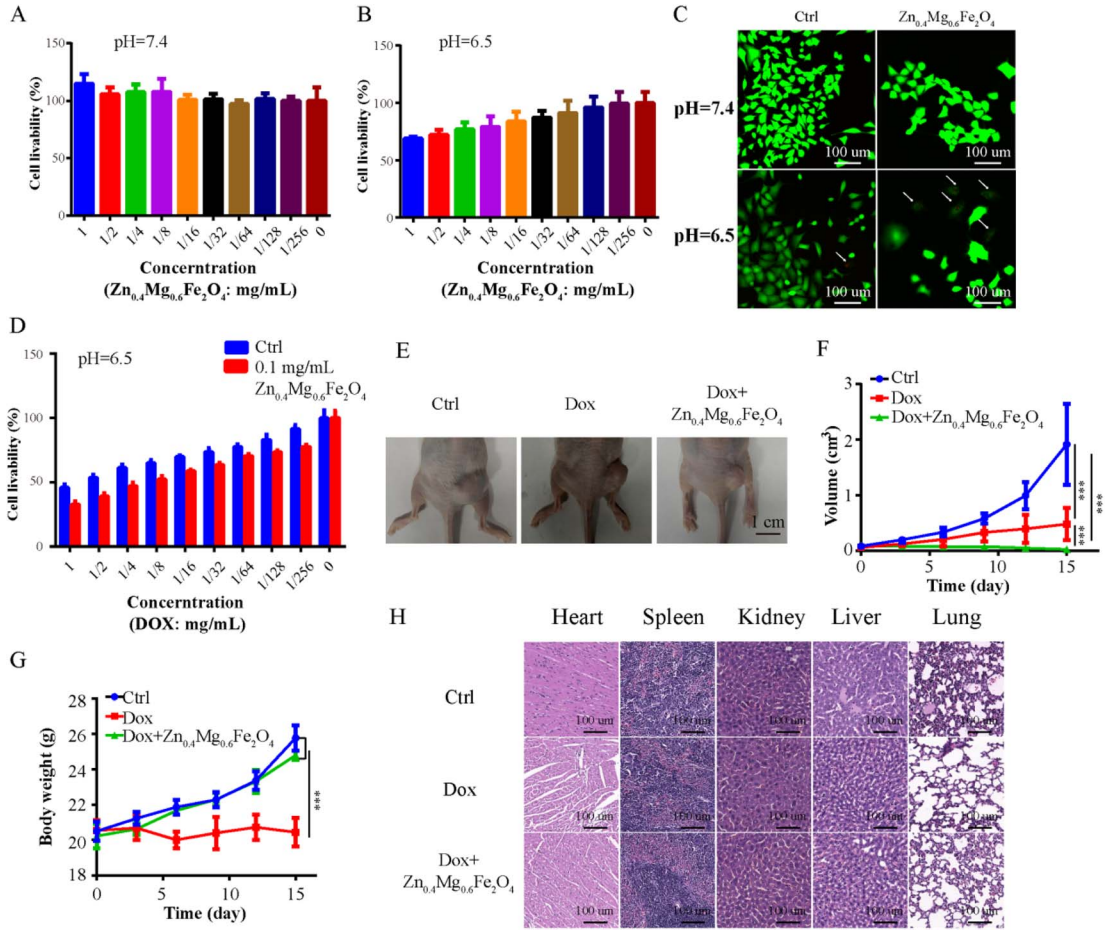

Fig. 7 $Zn_{0.4}Mg_{0.6}Fe_2O_4$ could enhance the chemotherapy effect in OSCC. CCK-8 assay showing the toxicity of different concentrations of $Zn_{0.4}Mg_{0.6}Fe_2O_4$ in OSCC cells (A) in a neutral environment and (B) in an acidic environment. (C) Double-staining assay for live/dead cells: toxicity of 0.1 mg mL^{-1} $Zn_{0.4}Mg_{0.6}Fe_2O_4$ in OSCC cells in neutral and acidic environments. (D) The influence of 0.1 mg mL^{-1} $Zn_{0.4}Mg_{0.6}Fe_2O_4$ on the toxicity of different concentrations of DOX in OSCC cells. (E and F) Comparison of *in vivo* therapeutic efficacy between DOX and DOX + $Zn_{0.4}Mg_{0.6}Fe_2O_4$. (G) Comparison of body weights of DOX and DOX + $Zn_{0.4}Mg_{0.6}Fe_2O_4$ treatments. (H) Comparison of *in vivo* systemic toxicity of DOX and DOX + $Zn_{0.4}Mg_{0.6}Fe_2O_4$. Note: ***: $P < 0.001$.

to 200 μL of solution B at 1.5 h and 3 h. Ten minutes after addition, $Zn_{1-x}Mg_xFe_2O_4$ was separated by centrifugation. UV-vis spectra were recorded to measure the remaining H_2O_2 by measuring the absorbance at 405 nm.

3.4 O_2 generation

The generation of O_2 was measured according to a method reported in the previous literature[22] with minor modifications. In summary, 4 mg of $Zn_{1-x}Mg_xFe_2O_4$ was incubated with 20 mL of PBS (pH = 5.8) containing 0.5 mM H_2O_2 at 37 °C. The dissolved O_2 concentration was monitored with an oxygen meter (HI9146, HANNA instruments, Korea) in real time at 60, 120, 180, 240, 300, 360, and 420 min.

3.5 POD-like activity detection

The TMB assay was used to detect the POD-like activity of $Zn_{1-x}Mg_xFe_2O_4$. In brief, 20 μg of $Zn_{1-x}Mg_xFe_2O_4$ was incubated in different buffers (pH 5.8 or pH 7.4) containing 1 mM TMB and 50 mM H_2O_2. POD-like activity was measured by detecting the absorbance at 625 nm at 30, 60, and 120 min.

3.6 GSH-like properties

GSH consumption, Fe^{2+} generation and Fe^{3+} depletion were investigated to detect GSH-like activity of $Zn_{0.4}Mg_{0.6}Fe_2O_4$.[19,22] To investigate the consumption of GSH, 475 μL of $Zn_{0.4}Mg_{0.6}Fe_2O_4$ (10 μg mL^{-1}) was incubated with 25 μL of GSH (4 mM) at 37 °C for 6 and 12 h. $Zn_{0.4}Mg_{0.6}Fe_2O_4$ was separated by centrifugation and the supernatant was collected for GSH measurement using the GSH kit (Beyotime Biotechnology). Finally, 10 μL of the supernatant was added to 100 μL of the reaction mixture from the GSH kit for 25 min and the concentration of GSH was measured by UV-vis spectroscopy at 410 nm. To investigate Fe^{2+} generation, different concentrations of $Zn_{0.4}Mg_{0.6}Fe_2O_4$ (0.01, 0.025, 0.05, 0.1, 0.25, and 0.5 mg mL^{-1}) were incubated with/without 4 mM GSH in different buffers (pH 5.8 or pH 7.4) at 25 °C for 1 h, then the solutions were centrifuged (15 000 rpm, 20 min) and the supernatant was collected. A 100-μL volume of

saturated 1, 10-phenanthroline solution was added to the supernatant. The absorbance at 512 nm was subsequently monitored. To investigate Fe^{3+} depletion, 10 μg mL^{-1} $Zn_{0.4}Mg_{0.6}Fe_2O_4$ was cultured with 4 mM GSH in acidic buffer (pH = 5.8) at 25 °C for 12, 24, 36, and 48 h. Then the Fe^{2+} generation was quantitatively analyzed according to the standard Fe^{2+} concentration absorbance curve, and the Fe^{3+} depletion was equal to the Fe^{3+} generation.

3.7 Cell culture

The OSCC cell line SCC9 was obtained from Fudan University (Shanghai, China); SCC9 cells were cultured in DMEM medium (Gibco) supplemented with 1% FBS (Sigma) in a humidified incubator at 37 °C with 5% CO_2. All the cell lines tested negative for mycoplasma contamination.

3.8 The detection of H_2O_2 concentration in tissues and cells

The H_2O_2 concentration in tissues and cells was measured using an H_2O_2 assay kit (S0038, Beyotime) according to the manufacturer's protocol. Specifically, for the detection of H_2O_2 in tumor tissues and normal tissues acquired from OSCC patients, tissue samples were first homogenized with lysis buffer supplied by the H_2O_2 assay kit (the ratio was 100 μL of lysate to 5 mg of tissues), and then centrifuged at 12 000 rpm for 5 min. All operations were performed on ice. The supernatant was collected for subsequent measurement of H_2O_2.

This study was conducted in accordance with the Declaration of Helsinki and was approved by the medical ethics committee of the Institute Affiliated Stomatology Hospital, Medical School of Nanjing University. Written informed consent was obtained from all patients. For extracellular and intracellular H_2O_2 measurement in tumor cells, SCC9 cells were first incubated in fresh culture medium in a normoxic environment (21% O_2), in fresh culture medium in a hypoxic environment (1% O_2), and in fresh culture medium supplemented with 100 μL of $Zn_{0.4}Mg_{0.6}Fe_2O_4$ in a hypoxic environment for 24 h. The culture medium was then harvested to determine the extracellular H_2O_2 concentration. Subsequently, cells were lysed in 100 μL of lysis buffer and supernatants, collected by centrifuging at 12 000×*g* for 10 min, and were used to determine the intracellular H_2O_2 concentration. The H_2O_2 concentration detection step was as follows: 50 μL of sample solution was incubated with 100 μL of reaction solution at room temperature for 30 min and then absorption at 560 nm was measured.

3.9 Detection of HIF-1α expression

HIF-1α protein expression was detected by the immunofluorescence assay. Specifically, 1×10^3 cells (SCC9) were seeded in glass bottom culture plates. After 24 h of culture, cells were cultured in a normoxic environment, hypoxic environment, and hypoxic environment supplemented with 100 μg mL^{-1} $Zn_{0.4}Mg_{0.6}Fe_2O_4$ for an additional 24 h. The cells were then fixed with 4% paraformaldehyde for 20 min and blocked with 5% BSA for 30 min at room temperature. Cells were incubated with the primary antibody HIF-1α (Cat no.: 66730-1-Ig, Proteintech) overnight at 4 °C. Dylight-conjugated anti-mouse IgG (647-conjugated anti-mouse IgG, Abcam, USA) was used as the secondary antibody. The nucleus was stained with DAPI (Beyotime, China) and observed under a confocal scanning system (Ti, NIKON).

3.10 Intracellular ROS detection

Intracellular ROS expression was detected using a reactive oxygen species assay kit (Beyotime, China). In summary, 1×10^3 cells (SCC9) were seeded in glass bottom culture plates. After 24 h of culture, cells were placed in a normoxic environment, a normoxic environment supplemented with 100 μg mL^{-1} $Zn_{0.4}Mg_{0.6}Fe_2O_4$, a hypoxic environment, and in a hypoxic environment supplemented with 100 μg mL^{-1} $Zn_{0.4}Mg_{0.6}Fe_2O_4$ for an additional 24 h. The DCFH-DA probe (10 μM) was then added to the cells and incubated for another 30 min at 37 °C. Cells were washed three times with PBS and monitored using a fluorescence microscope (Ti2, NIKON) with 488 nm excitation.

3.11 Cell wound healing assay and transwell cell migration assay

The migration ability of OSCC cells was determined by the cell wound healing assay and the transwell cell migration assay. For the cell wound healing assay, Ibidi Culture-Insert 2 wells were placed in 6-well plates, and then SCC9 cells were seeded for 24 hours before forming a 500-μm cell scratch on the cell layer surface. Next, cells were cultured with a fresh medium in a normoxic environment, a hypoxic environment, and a hypoxic environment supplemented with 100 μg mL^{-1} $Zn_{0.4}Mg_{0.6}Fe_2O_4$. Phase-contrast images were acquired at the time of the scratch and 24 h later. For the transwell cell migration assay, 100 μL of SCC9 was seeded in the upper chamber with 10% FBS in the lower chamber in a normoxic environment, a hypoxic environment, and a hypoxic environment supplemented with 100 μg mL^{-1} $Zn_{0.4}Mg_{0.6}Fe_2O_4$. Twenty-four hours later, the cells at the bottom of the filter were stained with crystal violet staining solution (Beyotime, China), and the cell numbers were counted in five fields by microscopy.

3.12 Cell proliferation assay

The proliferation ability of OSCC cells was determined using a CCK-8 cell proliferation assay kit (Beyotime). Briefly, 1×10^3 SCC9 cells were placed in a 96-well plate and cultured for 24 h. The culture medium was then replaced with fresh medium (pH 6.5 or pH 7.4) supplemented with a different concentration of $Zn_{0.4}Mg_{0.6}Fe_2O_4$ (0–1 mg mL^{-1}) or different concentrations of DOX (0–1 mg mL^{-1}). After 1 day of incubation, the culture medium was aspirated and treated cells were washed with PBS, before the addition of 10 μL of CCK8 solution to each well and incubated for an additional 2 hours at 37 °C. The absorbance of each well at 450 nm was then measured using an IMark enzyme mark instrument (Bio-Rad Inc., USA). The cell proliferation ability was calculated on the basis of the absorbance data.

3.13 Live/dead cell double staining assay

A Calcein-AM/PI double staining kit (Cat no.: 40747ES76, Yeasen, China) was used to detect live/dead cells. Briefly, 1×10^3

cells (SCC9) were seeded in glass bottom culture plates. After 24 h of culture, cells were cultured in a neutral environment, in a neutral environment supplemented with 100 μg mL^{-1} $Zn_{0.4}Mg_{0.6}Fe_2O_4$, in an acidic environment, and in an acidic environment supplemented with 100 μg mL^{-1} $Zn_{0.4}Mg_{0.6}Fe_2O_4$ for an additional 24 h. The cells were then washed with 1× assay buffer three times and incubated with 100 μL of detection buffer (5 μL of 2 mM Calcein-AM solution and 15 μL of 1.5 mM PI solution in 5 mL of assay buffer) for 15 min at 3 °C and observed under a confocal scanning system.

3.14 Animal model

BALB/c athymic nude mice were provided by the Comparative Medical Center of YangZhou University. All mice were housed under SPF conditions in which food, water, bedding, and cages were irradiated prior to use. All animal procedures were performed according to Nanjing University Laboratory Animal Care and Use Guidelines and the experiments were approved by the Nanjing University Animal Ethics Committee. To investigate antitumor efficacy, mice with subcutaneous OSCC xenografts were randomly divided into three groups ($n = 5$ for each group) when the tumor reached approximately 0.05 cm^3: (1) PBS group (intravenous injection of 100 μL of PBS), (2) DOX group (intravenous injection of 100 μL of PBS containing 0.25 mg kg^{-1} DOX) and (3) DOX + $Zn_{0.4}Mg_{0.6}Fe_2O_4$ group (intravenous injection of 100 μL of PBS containing 0.25 mg kg^{-1} DOX and 0.5 mg kg^{-1} $Zn_{0.4}Mg_{0.6}Fe_2O_4$). The drugs were administered every 3 days for 5 times and the tumor volumes/body weight were recorded simultaneously. Tumor volumes were calculated using the following formula: $V = 0.5ab^2$ (a: the longest diameter and b: the shortest diameter). To examine histological changes in the organs of the experimental mice, including the heart, liver, spleen, lung and kidney, 15 days after drug administration, organs were collected from mice and samples were embedded in paraffin. Subsequently, the paraffin-embedded tissue sections were stained with H&E and observed using a light microscope.

3.15 Statistical analysis

Statistical analysis was performed using SPSS statistical software (version 23.0; IBM) and GraphPad Prism (Version 6.0, GraphPad Software, La Jolla, CA, USA). Student's two-sided t-test was used to evaluate statistical significance differences between two groups and one-way ANOVA was used to evaluate statistical significance differences between three or more groups. MANOVA was used to analyze the repeated measured data. A P-value ≤ 0.05 was considered statistically significant.

4 Conclusions

$Zn_{0.4}Mg_{0.6}Fe_2O_4$ possessed optimal enzyme-like activity including CAT-like, POD-like, and GSH-like activity across the series of $Zn_{1-x}Mg_xFe_2O_4$ nanoenzymes in an acidic environment. Furthermore, $Zn_{0.4}Mg_{0.6}Fe_2O_4$ could effectively improve the efficacy of DOX chemotherapy in the treatment of OSCC and reduce cardiotoxicity. $Zn_{0.4}Mg_{0.6}Fe_2O_4$ could serve as a promising alternative chemosensitizer in the management of OSCC.

Author contributions

Liang Chen: conceptualization, data curation, and writing - original draft. Qingmei Kong: validation and formal analysis. Mingxing Tian: formal analysis and methodology. Qian Zhang: validation. Chengwan Xia: formal analysis and review & editing. Chao Deng: methodology, project administration, review & editing, funding acquisition, and supervision.

Conflicts of interest

The authors declare that they have no known competing financial interests or personal relationships that could have appeared to influence the work reported in this paper.

Acknowledgements

The authors gratefully acknowledge support for this research from the Key Research Project Fund of Wannan Medical College (WK2019ZF07), Open Project of Key Laboratory of Non-coding RNA Transformation Research of Anhui higher education institutes (RNA202001), and Young Talents Training Project of Wannan Medical College (wyqnyx202008).

References

1 H. Sung, J. Ferlay, R. L. Siegel, M. Laversanne, I. Soerjomataram, A. Jemal and F. Bray, *Ca-Cancer J. Clin.*, 2021, **71**, 209–249.
2 J. B. Epstein, J. Thariat, R. J. Bensadoun, A. Barasch, B. A. Murphy, L. Kolnick, L. Popplewell and E. Maghami, *Ca-Cancer J. Clin.*, 2012, **62**, 400–422.
3 R. L. Siegel, K. D. Miller and A. Jemal, *Ca-Cancer J. Clin.*, 2018, **68**, 7–30.
4 C. Holohan, S. Van Schaeybroeck, D. Longley and P. Johnston, *Nat. Rev. Cancer*, 2013, **13**, 714–726.
5 G. Semenza, *Cell*, 2012, **148**, 399–408.
6 E. Rankin and A. Giaccia, *Science*, 2016, **352**, 175–180.
7 Y. Lv, S. Zhao, J. Han, L. Zheng, Z. Yang and L. Zhao, *OncoTargets Ther.*, 2015, **8**, 1941–1948.
8 B. Wadsworth, R. Cederberg, C. Lee, N. Firmino, S. Franks, J. Pan, N. Colpo, K. Lin, F. Benard and K. Bennewith, *Cancer Lett.*, 2020, **493**, 31–40.
9 I. Robey, B. Baggett, N. Kirkpatrick, D. Roe, J. Dosescu, B. Sloane, A. Hashim, D. Morse, N. Raghunand, R. Gatenby and R. Gillies, *Cancer Res.*, 2009, **69**, 2260–2268.
10 V. Estrella, T. Chen, M. Lloyd, J. Wojtkowiak, H. Cornnell, A. Ibrahim-Hashim, K. Bailey, Y. Balagurunathan, J. Rothberg, B. Sloane, J. Johnson, R. Gatenby and R. Gillies, *Cancer Res.*, 2013, **73**, 1524–1535.
11 L. Gao, J. Zhuang, L. Nie, J. Zhang, Y. Zhang, N. Gu, T. Wang, J. Feng, D. Yang, S. Perrett and X. Yan, *Nat. Nanotechnol.*, 2007, **2**, 577–583.

12 J. Wu, X. Wang, Q. Wang, Z. Lou, S. Li, Y. Zhu, L. Qin and H. Wei, *Chem. Soc. Rev.*, 2019, **48**, 1004–1076.
13 J. Kim, H. Cho, H. Jeon, D. Kim, C. Song, N. Lee, S. Choi and T. Hyeon, *J. Am. Chem. Soc.*, 2017, **139**, 10992–10995.
14 K. Fan, J. Xi, L. Fan, P. Wang, C. Zhu, Y. Tang, X. Xu, M. Liang, B. Jiang, X. Yan and L. Gao, *Nat. Commun.*, 2018, **9**, 1440.
15 C. Liu, T. Wu, C. Liu, K. Chen, Y. Chen, G. Chen and S. Lin, *Small*, 2017, **13**, 1700278.
16 R. Subapriya, R. Kumaraguruparan, C. Ramachandran and S. Nagini, *Clin. Biochem.*, 2002, **35**, 489–493.
17 X. Lin, R. Zhu, Z. Hong, X. Zhang, S. Chen, J. Song and H. Yang, *Adv. Funct. Mater.*, 2021, **31**, 2101278.
18 A. Vernekar, D. Sinha, S. Srivastava, P. Paramasivam, P. D'Silva and G. Mugesh, *Nat. Commun.*, 2014, **5**, 5301.
19 J. Shen, T. W. Rees, Z. Zhou, S. Yang, L. Ji and H. Chao, *Biomaterials*, 2020, **251**, 120079.
20 J. Kurian and M. J. Mathew, *J. Magn. Magn. Mater.*, 2018, **451**, 121–130.
21 D. Ghanbari and M. Salavati-Niasari, *Korean J. Chem. Eng.*, 2015, **32**, 903–910.
22 S. Y. Yin, G. Song, Y. Yang, Y. Zhao, P. Wang, L. M. Zhu, X. Yin and X. B. Zhang, *Adv. Funct. Mater.*, 2019, **29**, 1901417.